

Article

Interaction between WC and Inconel 625 under Solid and Liquid State Sintering Conditions

Lorena Emanuelli *, Alberto Molinari and Massimo Pellizzari 

Department of Industrial Engineering, University of Trento, 38123 Trento, Italy; alberto.molinari@unitn.it (A.M.); massimo.pellizzari@unitn.it (M.P.)

* Correspondence: lorena.emanuelli@unitn.it

Abstract: Cobalt is the most used metal binder in hard metals since its extraordinary wetting, adhesion and mechanical properties. Nevertheless, it has been recognized genotoxic and cancerogenic with higher toxicity in combination with WC. To substitute Co with an alternative binder, the interaction between the binder and WC must be taken into account. In this work, IN625 is considered as a binder alternative due to its desirable combination of high-temperature strength and corrosion/oxidation resistance. A characterization of the interaction between WC and IN625 was carried out by means of Scanning Electron Microscopy (SEM), Energy Dispersive X-Ray Spectroscopy (EDXS) and X-Ray Diffraction (XRD). Depending on the sintering temperatures, different phases were evidenced at the WC–IN625 superalloy interface. From 1250 °C to 1300 °C, where solid-state sintering takes place, $(\text{Cr},\text{Mo})_{23}\text{C}_6$, W_2C and (Cr,W) solid solutions were detected. At a sintering temperature of 1350 °C, IN625 melts and the formation of additional phases, such as an intermetallic Ni_4W phase and (Mo,W) and (Mo,Nb) solid solutions, were observed. The precipitation of NbC and $(\text{Mo},\text{Cr})_{23}\text{C}_6$ carbides in IN625 was also detected.



Citation: Emanuelli, L.; Molinari, A.; Pellizzari, M. Interaction between WC and Inconel 625 under Solid and Liquid State Sintering Conditions. *Metals* **2021**, *11*, 666. <https://doi.org/10.3390/met11040666>

Academic Editors: Jose Torralba and Francisco Paula Gómez Cuevas

Received: 25 March 2021
Accepted: 16 April 2021
Published: 19 April 2021

Publisher's Note: MDPI stays neutral with regard to jurisdictional claims in published maps and institutional affiliations.



Copyright: © 2021 by the authors. Licensee MDPI, Basel, Switzerland. This article is an open access article distributed under the terms and conditions of the Creative Commons Attribution (CC BY) license (<https://creativecommons.org/licenses/by/4.0/>).

Keywords: sintering; tungsten carbide; Inconel 625; interface interaction; metal matrix composite

1. Introduction

WC-Co cemented carbides are the highest-performing tool materials due to their unique combination of hardness and toughness [1–3]. WC is the most used hard phase in cemented carbide due to its high hardness, appreciable plasticity and good wettability by liquid cobalt, which is fundamental to obtain a full density and a homogeneous distribution of the metallic binder after liquid phase sintering [1,4]. Even if Co is the most used metal binder in WC-Co due to its good mechanical properties and excellent wetting and adhesion, it has been recognized to be genotoxic and cancerogenic with higher toxicity in combination with WC [5]. Moreover, in applications where damage phenomena due to thermal fatigue, oxidation and corrosion may occur, a binder possessing a better high-temperature strength and corrosion/oxidation resistance than Co is necessary.

Many attempts have been made in the past to produce alternative cemented carbides with either complete or partial substitution of Co with Ni, Fe or Ru or with additions of modifiers, such as Ru, Cr or Mo [3,6–11]. The thermodynamic calculation of W-Ni-C and W-Co-C demonstrates that the solidus temperature and the WC solubility in the liquid are lower for the Ni-based system [12]. Guillermet [13] calculated a vertical section of W-Ni-C at 10 wt.% of Ni, obtaining a section similar to the one of W-Co-C at 10 wt.% of Co. In detail, the substitution of Co by Ni leads to the same width of the Ni-WC region but lower carbon content values. The increase in the C content in the WC-Ni region leads to a decreased melting temperature. Moreover, depending on the C content, the formation of a third phase, a $\text{M}_6\text{C}-\mu$ phase (low carbon) with graphite (high carbon), is predicted.

To obtain a hard metal with higher corrosion resistance, Motitschka et al. [14] studied the W-Co-Cr-C and W-Ni-Cr-C systems and measured the solubility of Cr in the solid binder. In W-Co-Cr-C, the maximum solubility is 5 wt.% Cr at 1000 °C, and a higher Cr content

led to the precipitation of the $(\text{Cr,Co,W})_7\text{C}_3$ carbide. In contrast, the maximum solubility in W-Ni-Cr-C was 7 wt.% Cr and, exceeding this value, Cr_3C_2 carbide forms. Even if WC has a lower wettability by liquid Ni than by liquid Co, and the solid solubility of WC into liquid Ni is not as high as for liquid Co, Ni seems to be a good alternative to Co because its similar interaction with W and C [12,13], and because of higher temperature strength.

Furthermore, in applications where high amounts of binder are necessary, namely hot rolling, the addition of Ni to Co binder leads to improved toughness [8]. Moreover, the addition of Cr increases the corrosion resistance of the W-Ni-C system. For these reasons, nickel-based superalloys represent an interesting alternative binder in high temperature applications due to their excellent combination of high-temperature strength and corrosion/oxidation resistance [10,11].

IN625 is a nickel-chromium alloy characterized by its high strength, outstanding corrosion resistance and service temperature up to 980 °C. It is a solid solution strengthening Ni superalloy due to the presence of Cr, Mo and Nb [15,16]. It is also characterized by precipitation hardening when either $\gamma^{\text{II}}\text{-Ni}_3\text{Nb}$, or a carbide like MC, M_6C and M_{23}C_6 precipitates are homogeneously distributed into the matrix [17]. Other intermetallic phases may create precipitates, including the $\delta\text{-Ni}_3\text{Nb}$ orthorhombic crystal structure and Laves A_2B -type hexagonal crystal structure. In addition, nitrides such as M_2N with a tetragonal crystal structure were detected [16–22].

To the authors' knowledge, the chemical interaction between Ni superalloy and WC has been poorly studied until now. Some investigations have been carried out on a composite produced by additive manufacturing and laser cladding [23–26]. Many different phases were detected, including WC, W_2C , MC, W_xC_y , M_{23}C_6 , Ni_xW_y , Ni_3Nb and Laves A_2B -type. Huebner et al. [24] studied the grain boundary interaction between IN625 and WC during laser metal deposition and revealed the presence of two major phases: $\text{Ni}_{0.85}\text{W}_{0.15}$ and $\text{Ni}_6\text{Mo}_6\text{C}_{1.06}$, indicating that WC grains dissolve into the Ni matrix. Three different IN625 (104 μm)–WC (0.54 μm) composites with 10, 20 and 30 wt.% of WC produced by powder laser cladding were investigated by Janicki and Musztyfaga [26]. Through XRD analysis, only Ni and WC were detected in IN625-WC with 10 and 20 wt.% of WC. In addition, W_2C , NbC, $(\text{Nb,W})\text{C}$, $\text{W}_6\text{C}_{2.54}$ and $(\text{W,Cr,Ni})_{23}\text{C}_6$ carbides were detected in the 30 wt.% WC composite. There is a paucity of research in terms of the production of WC–IN625 hard metals manufactured with the press and sinter technology.

The aim of this work is to investigate the interaction between WC and IN625 during sintering of a prior compacted powder. Large IN625 particles were used in order to obtain a wide and localized interface region to facilitate the analyses at the Scanning Electron Microscope (SEM). Conversely, the use of a fine/ultrafine Inconel powder, which is mandatory to achieve a homogeneous distribution of the metallic binder in the sintered microstructure, would result in a very thin and highly dispersed interface. A 70 wt.% WC–30 wt.% IN625 mix was processed by hot compaction and sintering at different temperatures. The high binder content was chosen to simulate the composition of hard metals for high temperature applications (e.g., hot rolls). It also helps in the investigation since it favors the formation of a large interface region between the two constituents. The microstructure and the phase constitution of samples were analyzed by Scanning Electron Microscopy (SEM), Energy Dispersive X-Ray Spectroscopy (EDXS) and X-Ray Diffraction (XRD).

2. Materials and Methods

Commercial WC and IN625 powders were used. The chemical composition of IN625 powder used in this study is summarized in Table 1.

Table 1. Chemical composition of the IN628 powder.

Chemical Composition of IN625 (wt. %)								
Ni	Cr	Mo	Nb	Fe	Si	Mn	O	C
64.81	21.30	8.90	3.58	0.42	0.41	0.38	0.06	0.01

The average particle size of WC is 0.8 μm , while that of IN625 is in the range of 53–150 μm . The powders were blended (70 wt.% WC and 30 wt.% of IN625) using a Turbula mixer. Disc samples (D 20 mm, H 10 mm) were hot-compacted with a pressure of 60 MPa at 950 $^{\circ}\text{C}$ for 5 min using a SPS-1050 system produced by Sumitomo Coal Mining Co. Ltd with punches covered by BN to avoid current flow through the powder. In this way, the powder was heated up only by conduction from the die.

A conventional sintering process in a tubular furnace was carried out in a N_2 atmosphere, using a heating and cooling rate of 4 $^{\circ}\text{C}/\text{min}$, and dwells of 30 min at 1250 $^{\circ}\text{C}$, 1275 $^{\circ}\text{C}$, 1300 $^{\circ}\text{C}$ and 1350 $^{\circ}\text{C}$. Temperatures were selected from the results of a Differential Temperature Scanning Calorimeter (DTSC) analysis. It was carried out in a N_2 atmosphere with a heating rate of 10 $^{\circ}\text{C}/\text{min}$ up to 1400 $^{\circ}\text{C}$.

The sintered samples were observed by SEM after a grinding and polishing with a 1- μm diamond suspension. The evolution of the interdiffusion region was evaluated by ImageJ software. The chemical concentration gradients in the interaction regions and the element mapping in IN625 were analysed by EDXS. In detail, a line scan of 25 μm across the interaction area was used to record one-dimensional concentration profiles for selected chemical elements. Quantitative phase analyses were performed by XRD using Italstructures IPD300 diffractometer (IPD3000/CPS120) equipped with an Intel CPS120 detector, and a $\text{Cu K}\alpha$ ($\lambda = 0.1541 \text{ nm}$) source of 1200 W with a beam size of $2 \times 8 \text{ mm}$. The sample was positioned in reflection geometry with a fixed omega angle of 5 degrees. The diffraction spectra were elaborated by the Rietveld method by MAUD software (Materials Analysis Using Diffraction) [27].

3. Results and Discussion

Figure 1 shows the DTSC curves of the IN625 powder and on the 70 wt.% WC–30 wt.% IN625 mix.

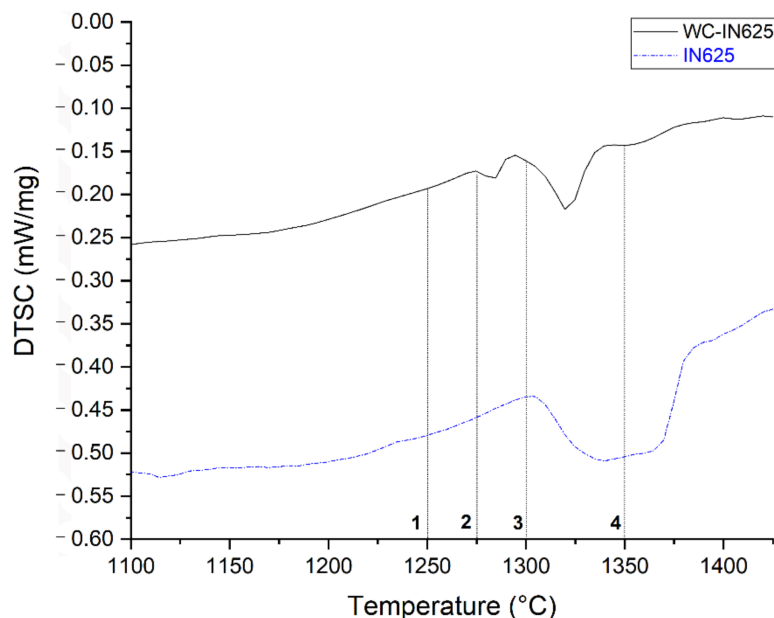


Figure 1. Differential Temperature Scanning Calorimeter (DTSC) curve of IN625 powder and of 70 wt.% WC–30 wt.% IN625 at a heating rate of 10 $^{\circ}\text{C}/\text{min}$.

The melting range of IN625 is between 1307 $^{\circ}\text{C}$ and 1380 $^{\circ}\text{C}$, with the peak at 1361 $^{\circ}\text{C}$. In the WC–IN625 mix, two endothermic peaks were detected. The first peak started at 1278 $^{\circ}\text{C}$ and finishes at 1284 $^{\circ}\text{C}$, and could refer to an endothermic reaction between WC and IN625 or to an incipient melting of IN625 in contact with WC, enhanced by the solubilization of C. No information was available about the effect of carbon on the melting temperatures of the superalloy, but it is well known that carbon in solid solution decreases

the melting temperature of Ni in the W-Ni-C phase diagram [3]. The second peak between 1311 °C and 1332 °C refers to the melting of IN625.

Based on the DTSC results, four different sintering temperatures were selected 1250 °C, 1275 °C, 1300 °C and 1350 °C. While the sintering process in cycles 1 and 2 is in a solid state, liquid-phase sintering occurs in cycle 4. In cycle 3, the formation of a small amount of liquid might be observed. The micrographs of the hot-compacted sample (pre-compacted) and of the sintered samples are shown in Figure 2.

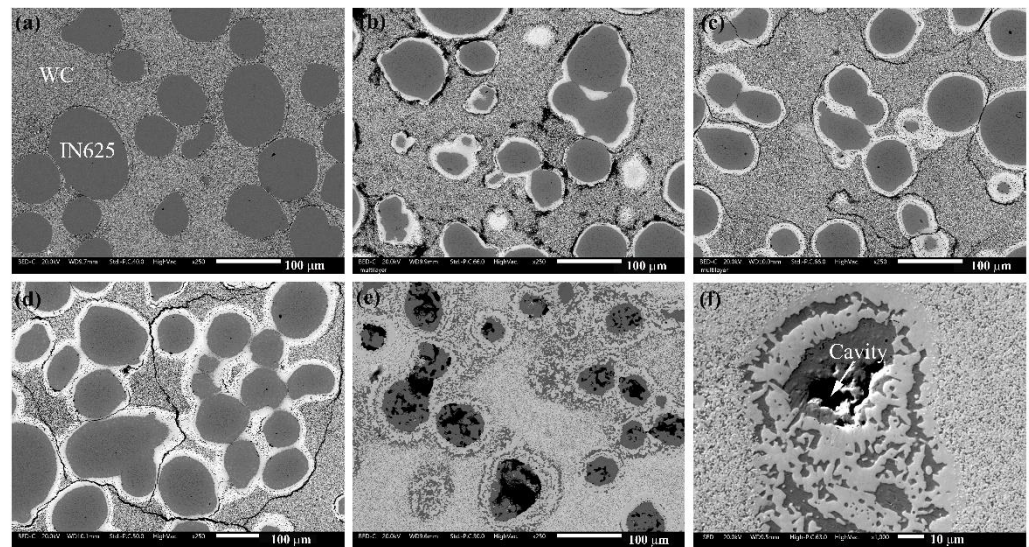


Figure 2. WC–IN625 microstructure of the pre-compacted (a), and sintered specimens at 1250 °C (b), 1275 °C (c), 1300 °C (d), 1350 °C (e,f).

From Figure 2 it is clearly evident that in pre-compacted form and after sintering at 1250, 1275 and 1300 °C, a high amount of cracks surrounded the IN625 powder due to the high difference between the WC and IN625 grain sizes. These cracks disappeared when the liquid-phase sintering occurred, as shown in Figure 2d. For the purposes of this work, large IN625 particles were selected to facilitate the analysis of the interaction between WC–IN625 leading to a material impossible to test mechanically. Figure 2 highlights that in the pre-compacted condition, the consolidation of the powders occurs without any reactions. Conversely, after the sintering cycles, an interdiffusion region (white area) surrounding the IN625 particles was observed, forming a shell with a thickness that increased with the increase of the sintering temperature, as shown in Figure 3.

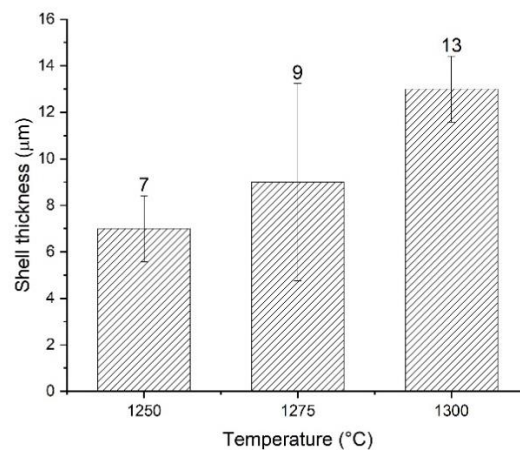


Figure 3. Shell thickness surrounding the IN625 powder after at 1250 °C, 1275 °C and 1300 °C.

A greater variation of the thickness was evident from 1275 °C to 1300 °C than from 1250 °C to 1275 °C. This could be justified by the formation of a liquid phase at 1300 °C that enhances the interdiffusion process. No morphological variations were observed between 1250 °C, 1275 °C and 1300 °C, suggesting that the interaction gave rise to the formation of the same products. This confirms that the first peak at 1284 °C observed in the DTSC curve of WC–IN625 mixture (Figure 1) refers to local melting of IN625 in contact with WC and not to the formation of different phases at lower temperatures. Liquid phase sintering takes place only in cycle 4, at the highest sintering temperature (1350 °C) where the superalloy is completely melted. In this condition, the microstructure of the interaction region is completely different since the melted superalloy had spread to the surrounding areas (Figure 2f).

The concentration profiles of the different elements through the interaction zones between WC and IN625 in the pre-compacted condition and after the four different sintering cycles are shown in Figure 4.

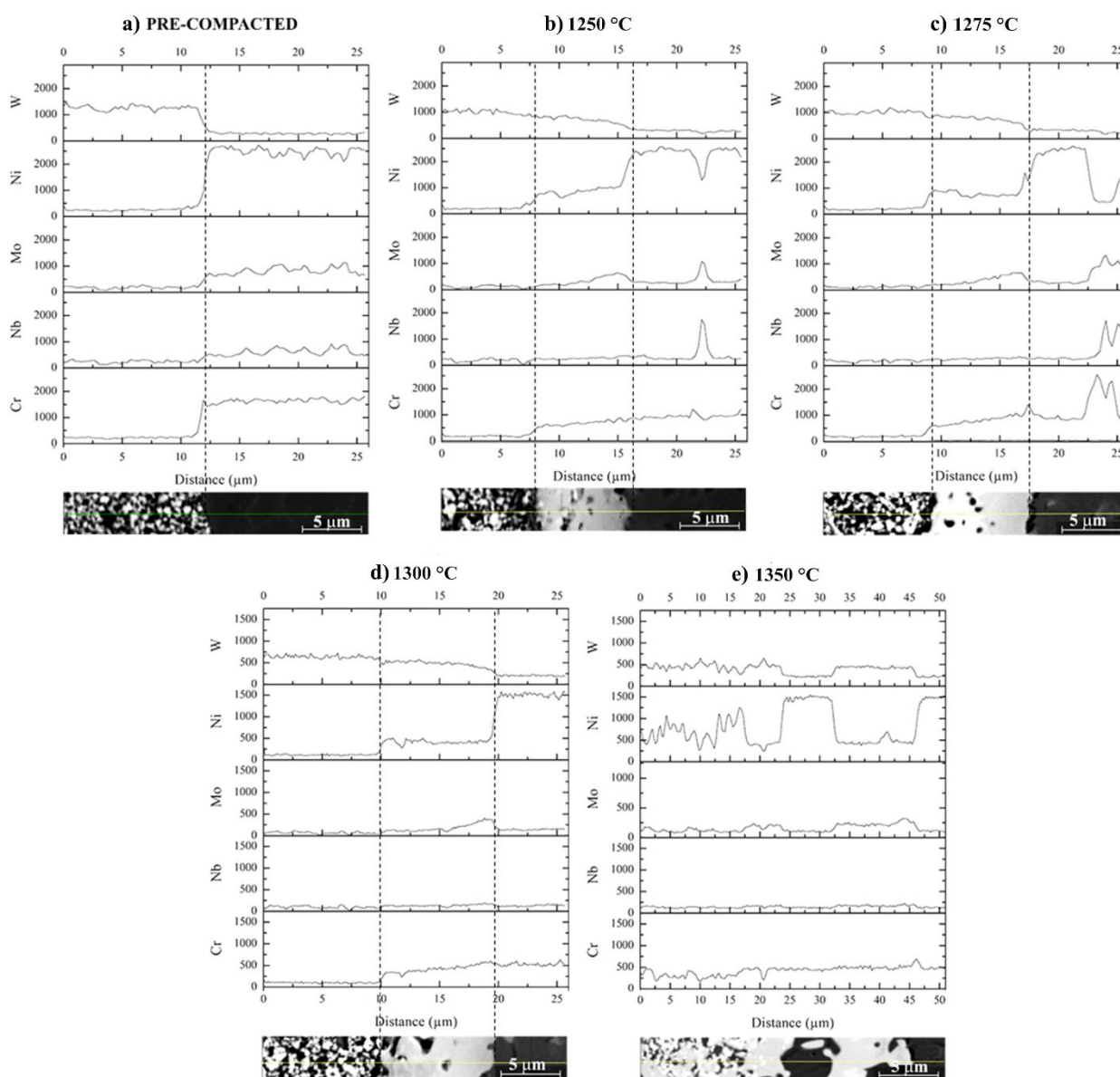


Figure 4. Line scan profiles of the different elements in the interaction area shown in the images, of WC–IN625 in the pre-compacted condition (a) and after sintering at 1250 °C (b), 1275 °C (c), 1300 °C (d) and 1350 °C (e).

Ni, Cr, Mo and Nb are obviously present in the IN625 powder. However, W is present in the WC particles area. The variation of the Cr, Mo and Nb inside IN625 particles will be analyzed later (Figure 6). Considering the interaction area between IN625 particle and WC carbides, in the pre-compacted condition, the concentration gradients are sharp, indicating that no diffusion phenomena occurred at the WC–IN625 interface. In the 1250 °C sintered specimen, an interdiffusion layer with a thickness of around 8 µm formed, confirming the shell thickness reported in Figure 3. The concentration profiles displayed a continuous and gradual variation of Cr and W elements. In contrast, Mo showed a concentration peak near the IN625, and Ni drastically decreased with a stepped trend in the interaction area. The Mo amount in the interdiffusion layer was higher than that in the IN625, suggesting the formation of a Mo-rich phase. Increasing the sintering temperature up to 1300 °C, the thickness of the interaction region increased and the concentration peak of Mo near the IN625 particle was confirmed.

During sintering at 1350 °C, IN625 melts and all the elements spread into the surrounding areas. The concentration profiles show that the black areas in the microstructure are rich of Ni (superalloy), which is different than those in the gray areas where W is the main element. Mo, Nb and Cr seemed to be homogeneously distributed. The Mo and Cr peaks in the same points highlighted the presence of a (Cr,Mo)-rich phase, perhaps a $(\text{Mo,Cr})_{23}\text{C}_6$ carbide.

To define the phases present after the different sintering cycles, Figure 5 shows the XRD spectra.

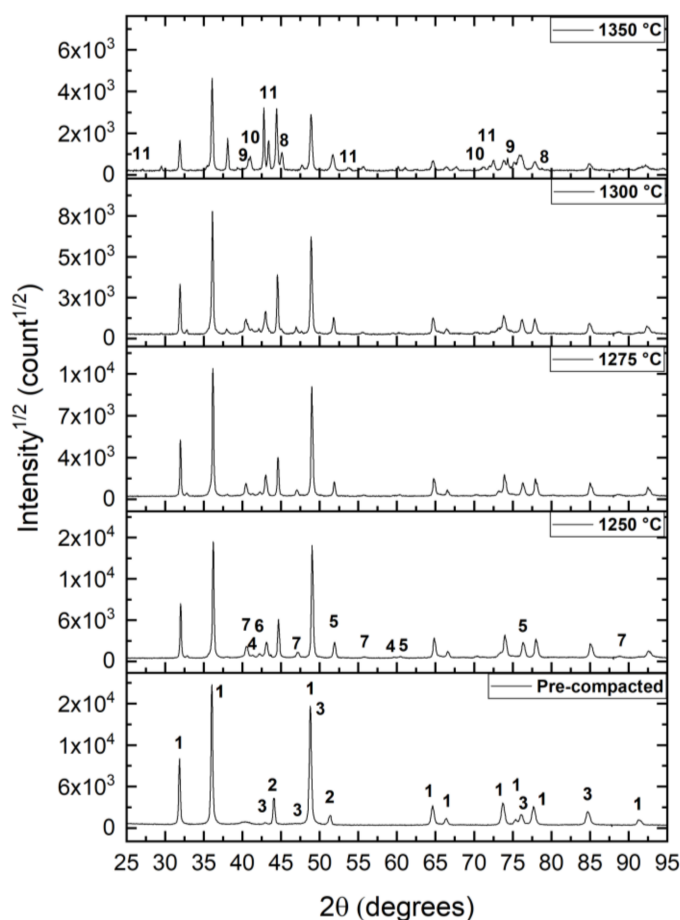


Figure 5. X-ray diffraction patterns of the 70 wt.% WC and 30 wt.% IN 625 mixture after compaction and sintering at different temperatures.

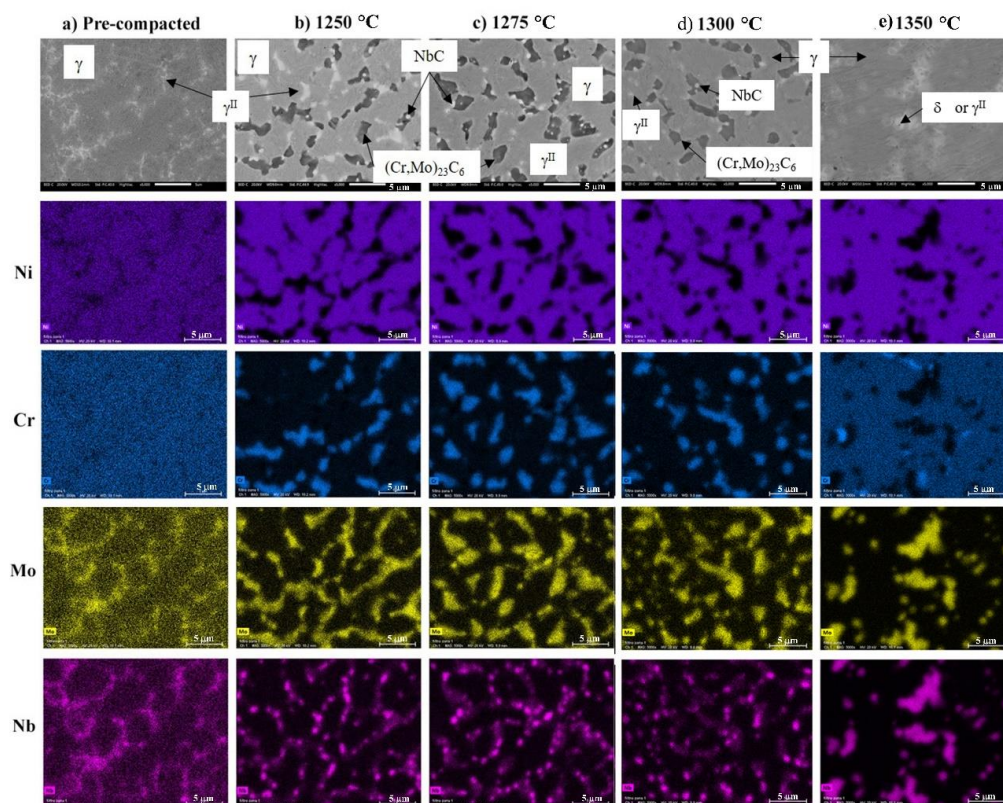
The results of the quantitative analysis of phases by MAUD are summarized in Table 2.

Table 2. Quantitative analysis obtained by MAUD of the phases present in different conditions.

Phase	MAUD Quantitative Analysis (vol.%)											
	WC	γ	Ni_3Nb (γ^{II})	NbC	W_2C	(Cr,W)	$(\text{Cr,Mo})_{23}\text{C}_6$	Ni_3Nb (δ)	(Mo,W)	(Mo,Nb)	Ni_4W	
Precomp	52	35	13	-	-	-	-	-	-	-	-	
1250 °C	30	29	11	2	1	1	26	-	-	-	-	
1275 °C	26	26	14	2	2	1	29	-	-	-	-	
1300 °C	20	30	16	2	2	1	29	-	-	-	-	
1350 °C	10	22	10	8	2	9	9	7	10	5	8	

In the pre-compacted specimen WC, γ and γ^{II} are the only phases detected, confirming the absence of any significant interaction at the interface [23]. The sintering cycles promote the formation of new phases in the interaction region and in IN625. In the spectra relevant to cycles 1, 2 and 3, the detected phases are WC, γ , γ^{II} , NbC, W_2C , (Cr,W) solid solution and $(\text{Cr,Mo})_{23}\text{C}_6$. The amount of these phases changes by increasing the sintering temperature: γ , NbC and (Cr,W) solid solution remain constant while the W_2C and $(\text{Cr,Mo})_{23}\text{C}_6$ carbides increase from 1250 °C up to 1275 °C and remain constant at 1300 °C. In addition, the WC amount decreased and the γ^{II} content increased by increasing the sintering temperature up to 1300 °C. The formation of Cr-rich phases is deleterious in terms of corrosion resistance since Cr must be homogeneously distributed to form a continuous passivation film on the surface. W_2C also had an embrittling phase, as observed in the WC-Co system [3]. NbC, with a small and rounded shape and a homogeneous distribution in the matrix, increased in terms of hardness and strength, as did the ordered precipitate γ^{II} . After sintering at 1350 °C, the amount of the mentioned phases changed and the formation of new phases, namely Ni_4W , δ and (Mo,W) and (Mo,Nb) solid solutions occurred, favored by the melting of IN625.

Figure 6 shows the microstructural evolution and the element mapping in the IN625 particle in the pre-compacted condition and after sintering at 1250 °C, 1275 °C, 1300 °C and 1350 °C.

**Figure 6.** Microstructure evolution and element mapping of IN625 powder after pre-compacted condition (a), and after sintering at 1250 °C (b), 1275 °C (c), 1300 °C (d) and 1350 °C (e).

Based on the XRD results (Table 2) and on the element mapping, it is possible to define the phase in IN625 in the different sintering conditions. The sintering process leads to a decrease of elements dissolved in the face centered cubic (fcc) γ matrix and to the precipitation of NbC and $(\text{Mo,Cr})_{23}\text{C}_6$ carbides in different sintering conditions [16–22]. NbC is rounded and homogeneously distributed in the matrix. The formation of MC and M_{23}C_6 carbides was caused by the decomposition of WC in W_2C and C, and the latter may react with Nb, Cr and Mo. When the liquid phase forms, only the fcc γ matrix, γ^{II} and/or the δ phase were detected. With element mapping, it was not possible to distinguish from γ^{II} and δ since both are characterized by the same chemical composition and differ only in term of crystalline structure.

The transformations occurring during the sintering processes at the different temperatures affected the lattice parameter of the fcc γ matrix, as reported in Table 3.

Table 3. Lattice parameter (a) of γ fcc (face centered cubic) crystal structure in the different conditions.

Ni-fcc	Pre-Compacted	Lattice Parameter of γ (Å)			
		1250 °C	1275 °C	1300 °C	1350 °C
a_γ	3.557	3.528	3.532	3.537	3.548

In pre-compacted conditions, the lattice parameter of the γ is 3.557 Å. The sintering process and the C diffusion into IN625 promoted the precipitation of Cr, Mo and Nb carbides that justified the decrease of the γ lattice parameter at 1250 °C [28,29]. The increase in the sintering temperature from 1250 °C to 1300 °C brings about increased γ lattice parameters due to the dissolution of WC and the consequent W enrichment of γ . In the liquid-phase sintering, the dissolution of a high amount of WC into a liquid phase led to the final enrichment of W into γ and the precipitation of Ni_4W .

From these results, it is clear that the effect of Cr and Mo on the solid solution hardening of the γ matrix decreased as the sintering temperatures increased. Nevertheless, W is a solid solution strengthening element. For this reason, the higher amount of W in solid solution in the γ matrix and the precipitation of γ^{II} and NbC are expected to increase the strength of the superalloy through solid solution and precipitation hardening, respectively.

4. Conclusions

The principal motivation for this work was to study the interaction between WC and IN625 superalloy to produce a Co-free cemented carbide with higher temperature strength and corrosion/oxidation resistance with respect to the conventional material. Preliminary analyses of the interaction between WC and IN625 during thermal cycles simulating sintering at temperatures between 1250 °C and 1350 °C were carried out. The results of this work allow for the following conclusions.

- Sintering at temperature up to 1300 °C. No liquid phase is formed. The interaction between WC and IN625 brings about the formation of W_2C , $(\text{Mo,Cr})_{23}\text{C}_6$ and solid solution (Cr,W). Increasing the sintering temperature, (Cr,W) solid solution remains constant and the W_2C and $(\text{Cr,Mo})_{23}\text{C}_6$ carbides increase from 1250 °C up to 1275 °C; above this temperature, they remain constant. Obviously, due to the diffusion process, the WC content decreases by increasing the sintering temperature.
- Sintering at 1350 °C. A liquid phase sintering forms that enhances the interaction between the constituents of the powder mix. Additional phases are formed, namely (Mo,W) and (Mo,Nb) solid solutions, and the intermetallic Ni_4W phase.
- In the IN625 microstructure, the sintering process leads to a decrease of solute contents in the fcc γ matrix and the precipitation of NbC and $(\text{Mo,Cr})_{23}\text{C}_6$ carbides under the investigated sintering conditions. An increased sintering temperature up to 1275 °C promotes the precipitation of $(\text{Mo,Cr})_{23}\text{C}_6$, while the amount of NbC remains constant. No composition variation of both carbides were observed when the sintering temperature was increased from 1275 °C and 1300 °C. In addition, the γ amount remains

quite constant and γ^{II} content increases by increasing the sintering temperature up to 1300 °C. When liquid-phase formation occurs, only the fcc γ matrix, γ^{II} and δ phase were detected.

Neither mechanical tests nor oxidation tests were carried out in this work. As such, the specimens must be produced by using fine IN625 particles to achieve a homogenous distribution of the metallic matrix in the sintered microstructure of the modified hard metal. However, the following conclusions can be drawn about the possible effect of the microstructural constituents produced during the sintering cycles:

1. γ^{II} and NbC are expected to affect mechanical properties positively by precipitation hardening;
2. The Cr-rich phases may also improve mechanical properties, but they should have a negative effect on the oxidation/corrosion resistance;
3. W_2C is an embrittling phase in WC-Co;
4. No reference in the literature was found about the effect of the (Mo,W) solid solution, (Mo,Nb), intermetallic Ni_4W phase, and δ .

Work is in progress to investigate these effects in a hard metal with a fine microstructure obtained by dispersing WC homogeneously in the metallic matrix. The results of the present work indicate that a low sintering temperature is needed to reduce the interaction between the two constituents. However, it will be interesting to investigate the properties of the material sintered at the highest temperature to verify the effect of the new phases and of their distribution in the microstructure resulting from the use of a fine IN625 powder.

Author Contributions: L.E., A.M., and M.P. conceptualized the research and contributed to data analysis, discussion of results, and paper writing. All authors have read and agreed to the published version of the manuscript.

Funding: This research received no external funding.

Conflicts of Interest: The authors declare no potential conflicts of interest with respect to the research, authorship, and/or publication of this article.

References

1. Brookes, K.J.A. *Hardmetals and other Hard Materials*; Metal Powder Industries Federation: Princeton, NJ, USA, 1992.
2. Santhanam, A.T.; Tierney, P.; Hunt, J.L. *Properties and Selection: Nonferrous Alloys and Special Purpose Materials*; ASM International: Materials Park, OH, USA, 1990.
3. Upadhyaya, G.S. *Cemented Tungsten Carbides: Production, Properties, and Testing*; Noyes Publications: Park Ridge, NJ, USA, 1998.
4. German, R.M. *Sintering Theory and Practice*; John Wiley & Sons, Inc.: New York, NY, USA, 1996.
5. Grilli, M.; Bellezze, T.; Gamsjäger, E.; Rinaldi, A.; Novak, P.; Balos, S.; Piticescu, R.; Ruello, M. Solutions for Critical Raw Materials under Extreme Conditions: A Review. *Materials* **2017**, *10*, 285. [[CrossRef](#)] [[PubMed](#)]
6. Penrice, T.W. Alternative Binder for Hard Metals. *J. Mater. Shaping Technol.* **1987**, *5*, 35–39. [[CrossRef](#)]
7. Bhaumik, S.K.; Upadhyaya, G.S.; Vaidya, M.L. Effect of Ti(C,N) addition on sintering behavior and properties of binder-modified WC-10Co cemented carbide. *J. Mater. Sci.* **1994**, *29*, 54–60. [[CrossRef](#)]
8. Roebuck, B.; Bennett, E.G.; Almond, E.A. Partitioning of molybdenum between carbide and binder phase in WC/Ni cemented carbides infiltrated with Ni-Cr-Mo alloys. *J. Mater. Sci. Lett.* **1986**, *5*, 473–474. [[CrossRef](#)]
9. Gonzalez, G.; Echeberria, J.; Sanchez, J.M.; Castro, F. WC-(Fe,Ni,C) Hardmetals with improved toughness through isothermal heat treatments. *J. Mater. Sci.* **1995**, *30*, 3435–3439. [[CrossRef](#)]
10. Waldorf, D.; Liu, S.; Stender, M.; Norgan, D. Alternative binder carbide tools for machining superalloys. In Proceedings of the International Conference on Manufacturing Science and Engineering, Evanston, IL, USA, 7–10 October 2008.
11. Tracey, V.A. Nickel in Hardmetals. *Int. J. Refract. Hard. Met.* **1992**, *11*, 137–149. [[CrossRef](#)]
12. Gabriel, A.; Pastor, H.; Deo, D.M.; Basu, S.; Allibert, C.H. New experimental data in the C-Fe-W, C-Co-W, C-Ni-W, C-Fe-Ni-W and C-Co-Ni-W cemented carbides systems and their application to sintering conditions. *Int. J. Refract. Hard. Met.* **1986**, *5*, 215–221.
13. Guillermet, A.F. Co-Fe-Ni-W-C phase diagram: A thermodynamic description and calculated sections for (Co-Fe-Ni) bonded cemented WC tools. *Z. Metallkd.* **1989**, *80*, 83–94.
14. Mankins, W.L.; Lamb, S. Nickel and Nickel Alloys. In *Properties and Selection: Nonferrous Alloys and Special-Purpose Materials*, 2nd ed.; ASM International: Materials Park, OH, USA, 1990; pp. 1362–1404.
15. Motitschka, R.; Etmayer, P.; Kny, E. Constitution of the Systems Co-Cr-W-C and Ni-Cr-W-C in the Cobalt and Nickel Corner. In Proceedings of the 12th International Plansee Seminar, Reutte, Austria, 8–12 May 1989; pp. 863–868.

16. Shankar, V.; Bhanu Sankara Rao, K.; Mannan, S.L. Microstructure and mechanical properties of Inconel 625 superalloy. *J. Nucl. Mater.* **2001**, *288*, 222–232. [[CrossRef](#)]
17. ASM International. *Properties and Selection: Nonferrous Alloy and Special-Purpose Materials*, 2nd ed.; ASM International: Materials Park, OH, USA, 1992; pp. 1362–1370.
18. Floreen, S.; Fuchs, E.G.; Yang, J.W. The Metallurgy of Alloy 625. In *Superalloy 718, 625, 706 and Various Derivatives*; Loria, E.A., Ed.; The Minerals, Metals & Materials Society: Pittsburgh, PA, USA, 1994; pp. 13–37.
19. Frank Rizzo, J.; Radavich, J. Microstructure characterization of PM 625-type materials. In *Superalloy 718, 625, 706 and Various Derivatives*; Loria, E.A., Ed.; The Minerals, Metals & Materials Society: Pittsburgh, PA, USA, 1991; pp. 297–308.
20. Petrzak, P.; Kowalski, K.; Blicharski, M. Analysis of phase transformations in Inconel 625 alloy during annealing. In Proceedings of the XXIII Conference on applied crystallography, Krynica Zdrój, Poland, 20–24 September 2015.
21. Dupont, J.N. Solidification of an Alloy 625 weld overlay. *Metall. Mater. Trans. A.* **1996**, *27*, 3612–3620. [[CrossRef](#)]
22. Cieslak, M.J. The solidification behavior of an Alloy 625/718 variant. In *Superalloy 718, 625, 706 and Various Derivatives*; Loria, E.A., Ed.; The Minerals, Metals & Materials Society: Pittsburgh, PA, USA, 1991; pp. 71–80.
23. Nguyen, Q.B.; Zhu, Z.; Chua, B.W.; Zhou, W.; Wei, J.; Nai, S.M.L. Development of WC-Inconel composites using selective laser melting. *Arch. Civ. Mech. Eng.* **2018**, *18*, 1410–1420. [[CrossRef](#)]
24. Huebner, J.; Kata, D.; Rutkowski, P.; Petrzak, P.; Kusiński, J. Grain-Boundary Interaction between Inconel 625 and WC during Laser Metal Deposition. *Materials* **2018**, *11*, 1797. [[CrossRef](#)] [[PubMed](#)]
25. Huebner, J.; Rutkowski, P.; Kata, D.; Kusinski, J. Microstructural and Mechanical Study of Inconel 625-Tungsten Carbide Composite Coatings Obtained by Powder Laser Cladding. *Arch. Metall. Mater.* **2017**, *2*, 531–538. [[CrossRef](#)]
26. Janicki, D.; Muszyfaga, M. Direct Diode Laser Cladding of Inconel 625/WC Composite Coatings. *J. Mech. Eng.* **2018**, *62*, 363–372. [[CrossRef](#)]
27. Rietveld, H.M. A profile refinement method for nuclear and magnetic structures. *J. Appl. Crystallogr.* **1969**, *2*, 65–71. [[CrossRef](#)]
28. Machado, I.F.; Girardini, L.; Lonardelli, I.; Molinari, A. The study of ternary carbides formation during SPS consolidation process in the WC–Co–steel system. *Int. J. Refract. Met. Hard Mater.* **2009**, *27*, 883–891. [[CrossRef](#)]
29. Li, S.; Wei, Q.; Shi, Y.; Zhu, Z.; Zhang, D. Microstructure Characteristics of Inconel 625 Superalloy Manufactured by Selective Laser Melting. *J. Mater. Sci. Technol.* **2015**, *31*, 946–952. [[CrossRef](#)]